

Middle to Late Pleistocene stability of the central East Antarctic Ice Sheet at the head of Law Glacier

M.R. Kaplan^{1*}, K.J. Licht², G. Winckler^{1,3}, J.M. Schaefer^{1,3}, N. Bader², C. Mathieson¹, M. Roberts⁴, C.M. Kassab², R. Schwartz¹, and J.A. Graly²

Division of Geochemistry, Lamont-Doherty Earth Observatory, Palisades, New York 10964, USA

ABSTRACT

Past behavior of outlet glaciers draining the East Antarctic Ice Sheet (EAIS) remains unresolved prior to Marine Isotope Stage 2 (MIS2). Study of blue ice moraines provides a relatively untapped approach to understand former EAIS activity. We focus on a blue ice moraine near Mount Achernar in the central Transantarctic Mountains, at the edge of the polar plateau. The well-preserved moraine consists of quasi-continuous or hummocky sediment ridges that form on top of upward-flowing, sublimating ice along the margin of Law Glacier. ¹⁰Be, ²⁶Al, and ³He cosmogenic nuclide ages on boulders from the ridges are coherent and in general are progressively older with distance from the relatively clean ice of the Law Glacier margin. Moraines closest to the Law Glacier margin postdate MIS2; farther away, they date to the last glacial cycle, and with more distance they are hundreds of thousands of years old. We conclude that cosmogenic dating of some blue ice moraines can provide age limits for changes at the heads of outlet glaciers that drain the central East Antarctic Ice Sheet, including prior to MIS2. Furthermore, the geomorphological, cosmogenic nuclide, and sedimentological evidence imply that the East Antarctic polar plateau adjacent to the central Transantarctic Mountains has been relatively stable for at least 200 k.y.

BACKGROUND

Knowledge of East Antarctic Ice Sheet (EAIS) behavior prior to Marine Isotope Stage 2 (MIS2) is commonly obtained from ice cores or indirectly from marine records or modeling (e.g., Petit et al., 1999; DeConto and Pollard, 2016) because of the scarcity of well-dated terrestrial deposits. Exceptions include dating of lateral moraines and drift sheets in the Dry Valleys (e.g., Sugden et al., 1993; Staiger et al., 2006) and elsewhere in the Transarctic Mountains, where more widely spaced studies have tended to focus on a million-year time scale, or the history of glacier thinning since MIS2 (e.g., Mercer, 1983; Ackert and Kurz, 2004; Bromley et al., 2010; Ackert et al., 2013; Joy et al., 2014). Observations from blue ice areas in the central Transantarctic Mountains, adjacent to the polar plateau, can be used to understand past changes in the central part of the EAIS. Blue ice ablation zones are common throughout the continental interior (Bintanja, 1999), yet moraines that form in these areas have received less attention than other geologic deposits around East Antarctica (Sinisalo and Moore, 2010). Recent studies in West Antarctica show that blue ice regions offer a dateable archive of former ice sheet behavior, especially prior to MIS2 (Fogwill et al., 2011; Hein et al., 2016).

Blue ice moraines form differently than temperate ice-marginal moraines where melting dominates. Prior studies have documented the processes that lead to sediment accumulations associated with blue ice areas (e.g., Whillans and Cassidy, 1983; Chinn, 1991, 1994; Cassidy et al., 1992; Sinisalo and Moore, 2010; Fogwill et al., 2011; Campbell et al., 2013; Hein et al., 2016; Bader et al., 2017). As the EAIS encounters the Transantarctic Mountains (Fig. 1), the barrier to flow causes ice convergence into outlet glaciers. Such settings are favorable for blue ice regions, where enhanced wind scouring and sublimation along glacier margins enables upward flow, which carries sediment to the surface (see the GSA Data Repository¹). Until recently, around the continent, it has

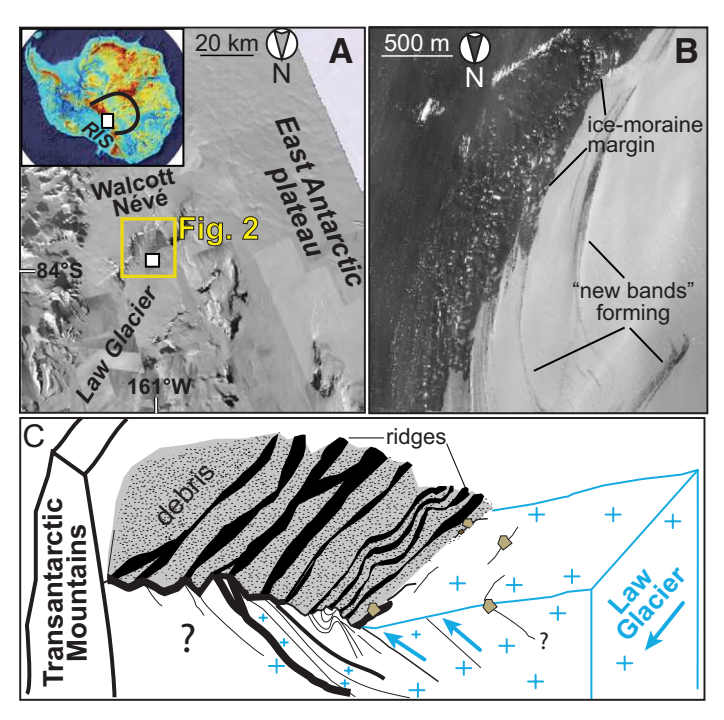


Figure 1. A: Location of Mount Achernar moraine at the head of the Law Glacier (East Antarctica). Panel B is within the small white box. In inset, color gradient shows bedrock elevation (red = high), and black line marks sector that drains through central Transantarctic Mountains (Fretwell et al., 2012). RIS—Ross Ice Shelf. B: Moraineice marginal zone, on DigitalGlobe (www.digitalglobe.com) image. C: Schematic cartoon, which is provided to help visualize how sediments may accumulate at Mount Achernar (Bader et al., 2017) (see Data Repository [see footnote 1]). Variable size of upward-flowing debris pathways reflects differential thickness. Question marks refer to lack of knowledge of subsurface.

²Department of Earth Sciences, Indiana University-Purdue University Indianapolis, Indianapolis, Indiana 46202, USA

³Department of Earth and Environmental Sciences, Columbia University, New York, New York 10027, USA

⁴2 Finch Street, Albert Town, Wanaka 9382, New Zealand

^{*}E-mail: mkaplan@ldeo.columbia.edu

¹GSA Data Repository item 2017324, supplemental text, figures, and tables, is available online at http://www.geosociety.org/datarepository/2017/ or on request from editing@geosociety.org.

remained poorly known for how long sediment accumulations have persisted on top of blue ice.

An important concept is that even after their initial formation, blue ice moraines still overlie glacier ice, and upward-flowing debris can cause continued accumulation near the surface (Fig. 1; Fig. DR1 in the Data Repository). Substantial removal of the underlying glacier ice would result in a reversal or change in gradient and flow, which should deform or even "drain" these surface sediments (e.g., Chinn, 1991, 1994; Fogwill et al., 2011; Hein et al., 2016). Conversely, a substantial increase in glacier thickness could eventually deform or displace the moraines, as perhaps observed in some areas (Chinn, 1991, 1994).

To assess past stability of the East Antarctic interior, we studied a well-preserved extensive blue ice moraine linked with Law Glacier, near Mount Achernar at the edge of the polar plateau, between the Queen Alexandra and Queen Elizabeth Ranges (Figs. 1 and 2). In this region, East Antarctic ice is sourced mainly from the Dome A sector, and it encounters the Transantarctic Mountains on the south and southwest sides of Mount Achernar (Fig. 1), where it splits into Law Glacier and Walcott Névé. Walcott Névé is slow-moving ice, a small part of which flows into the Lewis Cliff Ice Tongue (Fig. 2). Approximately 20 km down flow of Walcott Névé, the slower-moving ice converges back into Law Glacier (Fig. 1).

The Mount Achernar moraine consists of a series of troughs and ridges 1–12 m high that roughly parallel the form of the relatively clean Law Glacier margin, over an inland expanse of ~5 km (Figs. 2 and 3). The moraine overlies sediment-laden ice, and changes in surface elevation are overall on the order of tens of meters (Fig. 3) (Scarrow et al., 2014; Bader et al., 2017). Till thickness increases from <5 cm to >1 m with distance from the relatively clean surface of Law Glacier (Scarrow et al., 2014). Bader et al. (2017) used till provenance to understand better the nature of sediment accumulation at this site. They showed that distinct lithological bands can be observed quasi-continuously along ridges, for >5 km in places, and changes over time can be related to the location of subglacial erosion (Fig. DR1; Fig. 2A). The length of time the sediments have been exposed at the Mount Achernar moraine has remained largely unconstrained (Scarrow et al., 2014; Sun et al., 2015; Bader et al., 2017), except for a preliminary study by Hagen (1995) that indicated at least some exposure ages were >100 ka (Fig. 2).

RESULTS

To obtain an age framework for the moraine at Mount Achernar, we measured ¹⁰Be and ²⁶Al in sandstone and ³He in dolerite boulders (see the Data Repository). Our sampling strategy was to follow closely a topographic profile that is along a well-preserved part of the moraine, roughly perpendicular to ridge crests (Fig. 2; see the Data Repository). We sampled far (several kilometers) from the headwalls to avoid materials with a significant amount of pre-exposure. Within ~2 km of the clean surface of the Law Glacier margin, apparent exposure ages are ca. 5-20 ka (≤MIS2). Approximately 2 km to ~2.5 km from Law Glacier, apparent boulder ages are ca. 35 ka to ca. 100 ka (i.e., the last glacial cycle). Beyond ~2.5 km, all three nuclides yield ages ≥100 ka. Approximately 2.5-3.5 km away from the Law Glacier margin, boulders date from ca. 100 ka to ca. 200 ka. Also, on the southern end of the area, we dated two samples (MAR-11-48, MAR-11-52) left by northward-flowing local ice, which are also >100 ka (Fig. 2A). All three nuclides, ¹⁰Be-²⁶Al-³He, are in agreement that there is a net increase in age well into the hundredthousand-year time scale, at least until ca. 200 ka (Fig. 3B), regardless of minor age reversals that are discussed further below.

In addition, we show an unpublished ¹⁰Be-²⁶Al data set from Hagen (1995) (see the Data Repository). The recalculated ages, using present method systematics, are consistent with our findings, with the exception of one young outlier of 15 ka that is ~4 km from the Law Glacier (Fig. 2A). Hagen (1995) assumed this ca. 15 ka outlier could be explained by persistent snow in the depressed area where he collected the sample, and we do

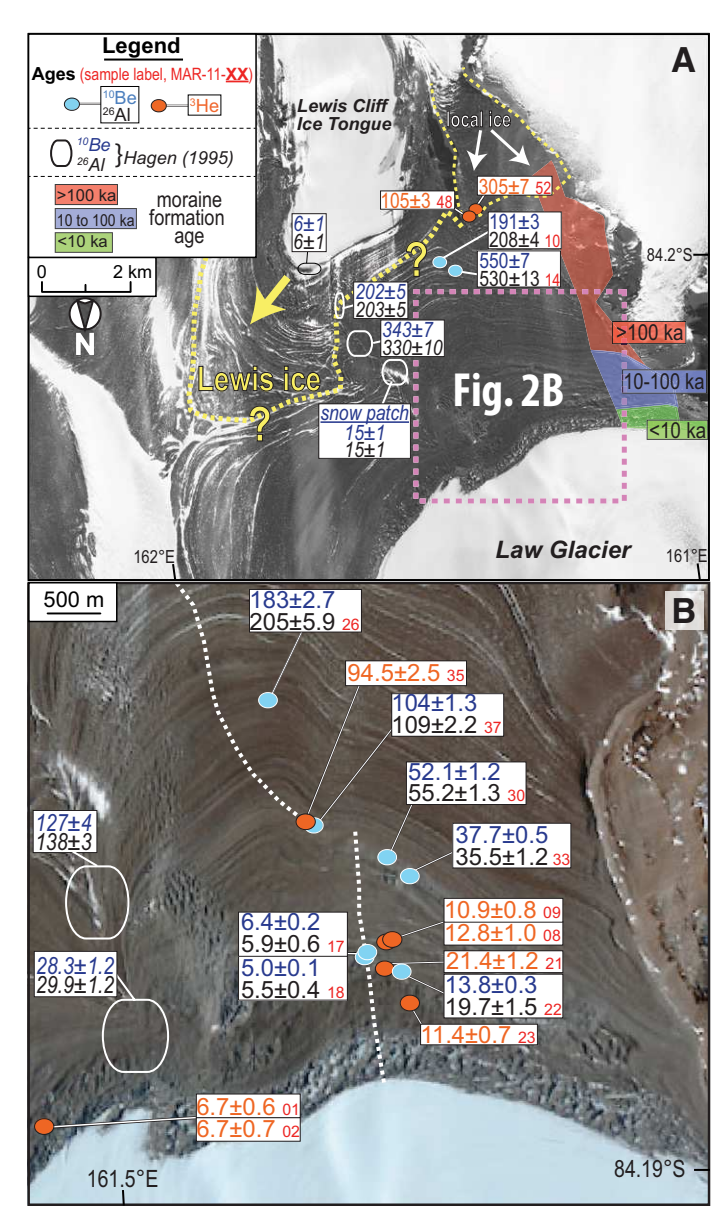


Figure 2. Blue ice moraine dating at Mount Achernar, East Antarctic Ice Sheet. A: DigitalGlobe (www.digitalglobe.com) image with locations of ¹⁰Be-²⁶Al (measured on same sample) and ³He ages (in ka), with analytical errors (±10).The 105 ka and 305 ka ages are on samples from northward-flowing local ice. Boundary between Law Glacier and Lewis Cliff Ice Tongue ice is marked in yellow, which is uncertain in places (question mark). B: Focus on north side of moraine. Dashed white line represents topographic profile in Figure 3 (from Bader et al., 2017); its orientation changes at ~2.4 km from glacier margin to follow center of well-preserved part of moraine.

not discuss it further. It is not possible to line up precisely Hagen's (1995) sample positions along our profile, given inexact locations (Figs. 2 and 3).

DISCUSSION AND CONCLUSIONS

The Mount Achernar blue ice moraine and its setting contain a valuable record of regional ice sheet history (Fig. 1). The ¹⁰Be-²⁶Al-³He ages progressively increase with distance away from the relatively clean Law Glacier margin (Fig. 3B). General ²⁶Al and ¹⁰Be age accordance (Fig. DR5) implies that the samples did not experience prolonged periods of burial (e.g., >100,000 yr) and re-exposure. Significant pre-exposure of ¹⁰Be may exist, for example, if the samples were originally rockfall from headwalls. However, for headwall material to exist where we sampled,

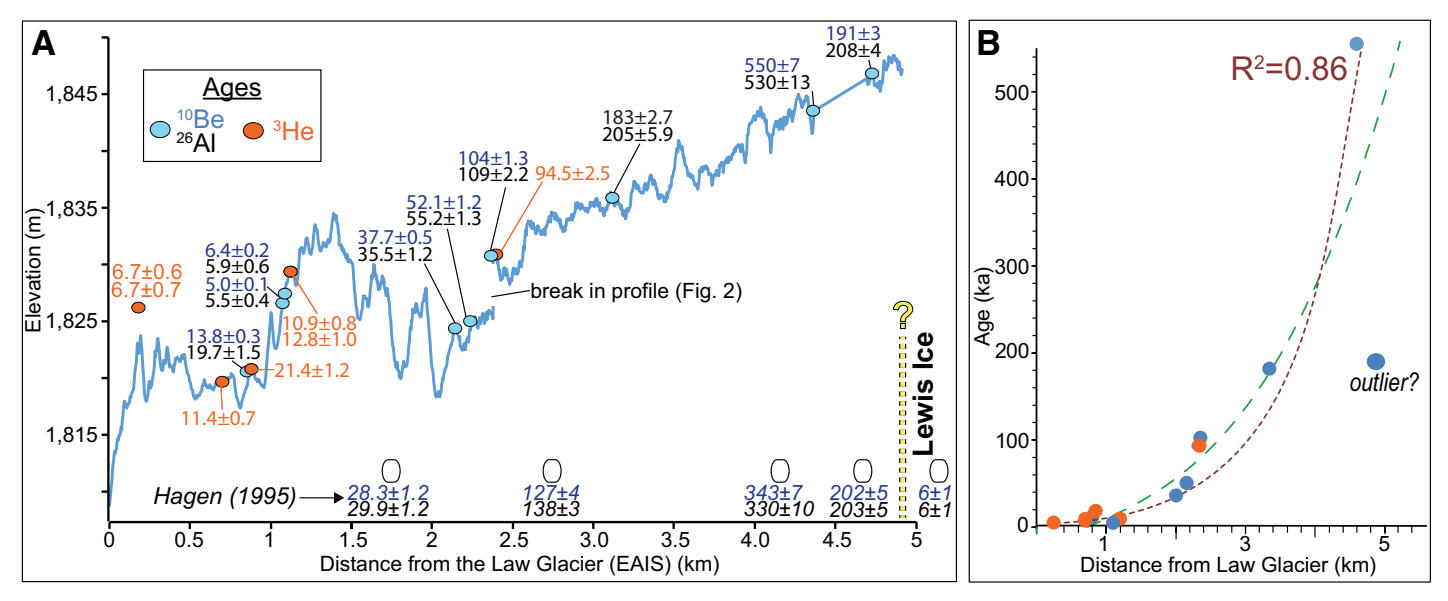


Figure 3. Net age increases away from modern Law Glacier, East Antarctic Ice Sheet (EAIS). A: Ages (in ka) plotted along topographic profile (see Fig. 2B) between Law Glacier and Lewis Cliff Ice Tongue ice (yellow line). For comparison, at estimated positions, we show the 6.7 ± 0.7 ka ³He age and ¹⁰Be-²⁶Al ages from Hagen (1995), except for 15 ka age (see text), which date samples to the east of the topographic profile (Fig. 2B). B: Exponential (green, long dashed) and second-order polynomial (brown, short dashed) fits are merely to show net age increase to at least ~3.5 km from Law Glacier (ca. 200 ka), and >5 km if we assume farthest dated sample, 191 ka (~5.6 km), is an outlier (see text). Errors are within symbol size.

debris would have had to have been transported against both the direction of ice flow and lateral accretion of moraine (Fig. 2A). Also, Mount Achernar is adjacent to the polar plateau, and hence there are limited upflow nunatak sources to provide rocks with pre-exposure.

The strong exposure age–distance trend shown in Figure 3B leads us to speculate that after boulders reach the surface along upward-flowing ice, they must remain somewhat stable above the thickening till (Scarrow et al., 2014; Bader et al., 2017). The age-distance progression also indicates that debris accretes laterally over time, and underlying sublimation decreases, which is consistent with the provenance-based interpretation of Bader et al. (2017) and conceptual model shown in Figure 1. Our findings are also consistent with quantitative measurements of salt accumulation (Graly et al., 2016). Specifically, the cosmogenic ages show a remarkably strong relationship ($R^2 = 0.99$) with the steady buildup of salt concentration (e.g., boron) by atmospheric deposition on the moraine surface (Graly et al., 2016).

Concerning the minor age reversals, these are discussed further because they may provide additional insight into formation of blue ice moraines. First, two samples have been exposed for less time, ~6-5 k.y. (at ~1.1 km), than boulders closer to Law Glacier (Fig. 2). We offer two possible scenarios that could cause the 6-5 ka exposure ages. Any explanation must adhere to the observation that these boulders have pristine tops with glacial striations, indicating negligible surface erosion (Fig. DR2). Periglacial processes may have been more active in this particular spot, which rotated both sampled boulders, exposing former underlying sides, by a similar amount. Alternatively, perhaps the younger 5-6 ka ages at ~1.1 km reflect the general age of the moraine surface and can be explained by the local emergence of younger sediment, possibly due to a contorted underlying ice structure (cf. as described in Chinn, 1991, 1994). Bader et al. (2017) presented findings (Fig. DR1) that are consistent with debris still being brought to the surface after initial formation of a debris layer (cf. Mackay and Marchant, 2016). Regardless of the cause, this minor age reversal does not negate the fact that the surface sediment generally increases in age away from the Law Glacier margin (Fig. 3B).

An age reversal also occurs in the older part of the sequence (Fig. 2). The 191 ka ¹⁰Be (208 ka ²⁶Al) age could be too young due to periglacial

processes or emergence of a younger boulder, or the 550 ka ¹⁰Be (530 ka ²⁶Al) age could be too old due to recycling of a boulder with prior exposure. However, the 550 ka boulder is surrounded by more weathered sediments compared with the younger part of the sequence (Fig. DR2D), documenting qualitatively that this area of the moraine is indeed older. In agreement with this interpretation, the highest boron salt concentration measured in the Mount Achernar moraine is near the 550 (530) ka boulder, supporting that this is the oldest part of the sequence (Graly et al., 2016). We also speculate that the ca. 200 ka age from Hagen (1995) could be originally from the northward-flowing Lewis Cliff Ice Tongue (dashed yellow line in Fig. 2) and was later reworked into Law-derived moraine. However, we emphasize, again, that any of these scenarios are consistent with our conclusions: beyond ~2.5 km from Law Glacier, the deposits are at least 100 ka, and beyond 3 km they are ca. 200 ka or older (Figs. 2 and 3).

In summary, a dateable, well-preserved, laterally extensive and quasi-continuous blue ice moraine sequence exists at Mount Achernar. The geomorphology of the sequence and coherent age progression (Figs. 2 and 3B) of three isotopes, ¹⁰Be-²⁶Al-³He, lead us to agree with prior studies that blue ice moraines represent quasi-equilibrium forms (Fogwill et al., 2011). Specifically, at the head of Law Glacier, well-preserved and extensive ridges have persisted for well into the hundred-thousand-year time scale. The age progression also provides a temporal foundation for understanding the process by which these and other blue ice moraines form.

Our findings are not compatible with this section of the interior EAIS undergoing marked lowering over the time represented (Fig. 1). The largest elevation changes in the moraine morphology (Fig. 1) are only on the order of tens of meters (Fig. 3A). If a non-equilibrium situation occurred at Mount Achernar, such as the loss of underlying ice or the buttressing effect of Law Glacier, we infer that this disruptive event should have distorted or even gutted the blue ice moraine (Fig. 3; Fig. DR1). Other recent sediment provenance and geochemical studies at this site are also consistent with relative stability of the EAIS near the head of Law Glacier over the time represented (Bader et al., 2017; Graly et al., 2016).

More broadly, we demonstrate that at least some blue ice moraines in the central Transantarctic Mountains can be dated into the hundredthousand-year time scale. Because these moraine sequences are fed by outlet glaciers connected to the nearby unconstrained EAIS plateau, they can be used to place limits on former ice flow, surface elevations, and thus model results for time periods such as MIS2 and prior (Sinisalo and Moore, 2010; Fogwill et al., 2011). For example, numerical models do not simulate much change where ice encounters the central Transantarctic Mountains, including during MIS2 when >500 m of surface change occurred where Law Glacier entered the Ross Sea embayment (e.g., Mercer, 1983; Bromley et al., 2010). We conclude that the EAIS in the area of the central Transantarctic Mountains has changed little through the last one or two glacial-interglacial cycles, even if major changes occurred elsewhere over the time period represented (DeConto and Pollard, 2016).

ACKNOWLEDGMENTS

We acknowledge support from National Science Foundation grants ANT-0944475, 0944578, and 1443213. We thank Spencer Niebuhr and the Polar Geospatial Center for imagery (Fig. 1B), Joe Petit, the New York Air National Guard, Raytheon, Michael Wolovick, and David Sugden and two anonymous reviewers for substantially improving the manuscript. This is Lamont-Doherty Earth Observatory Contribution #8131.

REFERENCES CITED

- Ackert, R.P., Jr., and Kurz, M.D., 2004, Age and uplift rates of Sirius Group sediments in the Dominion Range, Antarctica, from surface exposure dating and geomorphology: Global and Planetary Change, v. 42, p. 207–225, doi:10.1016/j.gloplacha.2004.02.001.
- Ackert, R.P., Jr., Putnam, A.E., Mukhopadhyay, S., Pollard, D., DeConto, R.M., Kurz, M.D., and Borns, H.W., Jr., 2013, Controls on interior West Antarctic Ice Sheet elevations: Inferences from geologic constraints and ice sheet modeling: Quaternary Science Reviews, v. 65, p. 26–38, doi:10.1016/j.quascirev.2012.12.017.
- Bader, N.A., Licht, K.J., Kaplan, M.R., Kassab, C., and Winckler, G., 2017, East Antarctic ice sheet stability recorded in a high-elevation ice-cored moraine: Quaternary Science Reviews, v. 159, p. 88–102, doi:10.1016/j.quascirev.2016 12.005
- Bintanja, R., 1999, On the glaciological, meteorological, and climatological significance of Antarctic blue ice areas: Reviews of Geophysics, v. 37, p. 337–359, doi:10.1029/1999RG900007.
- Bromley, G.R.M., Hall, B.L., Stone, J.O., Conway, H., and Todd, C.E., 2010, Late Cenozoic deposits at Reedy Glacier, Transantarctic Mountains: Implications for former thickness of the West Antarctic Ice Sheet: Quaternary Science Reviews, v. 29, p. 384–398, doi:10.1016/j.quascirev.2009.07.001.
- Campbell, S., Balco, G., Todd, C., Conway, H., Huybers, K., Simmons, C., and Vermeulen, M., 2013, Radar-detected englacial stratigraphy in the Pensacola Mountains, Antarctica: Implications for recent changes in ice flow and accumulation: Annals of Glaciology, v. 54, p. 91–100, doi:10.3189/2013AoG63A371.
- Cassidy, W., Harvey, R., Schutt, J., Disle, G., and Yanai, K., 1992, The meteorite collection sites of Antarctica: Meteroritics, v. 27, p. 490–525, doi:10.1111/j .1945-5100.1992.tb01073.x.
- Chinn, T.J., 1991, Polar glacier margin and debris features: Memorie della Societa Geologica Italiana, v. 46, p. 25–44.
- Chinn, T.J., 1994, Glacier disequilibrium in the Convoy Range, Transantarctic Mountains, Antarctica: Annals of Glaciology, v. 20, p. 269–276, doi:10.3189 /172756494794587122.
- DeConto, R.M., and Pollard, D., 2016, Contribution of Antarctica to past and future sea-level rise: Nature, v. 531, p. 591–597, doi:10.1038/nature17145.

- Fogwill, C.J., Hein, A.S., Bentley, M.J., and Sugden, D.E., 2011, Do blue-ice moraines in the Heritage Range show the West Antarctic ice sheet survived the last interglacial?: Palaeogeography, Palaeoclimatology, Palaeoecology, v. 335–336, p. 61–70, doi:10.1016/j.palaeo.2011.01.027.
- Fretwell, P., et al., 2012, Bedmap2: Improved ice bed, surface and thickness datasets for Antarctica: The Cryosphere, v. 7, p. 375–393, doi:10.5194/tc-7-375-2013.
- Graly, J., Licht, K., and Kaplan, M., 2016, Borate soil concentrations as an exposure age chronometer in Antarctic blue ice moraines: Geological Society of America Abstracts with Programs, v. 48, no. 7, doi:10.1130/abs/2016AM-283425.
- Hagen, E.H., 1995, A geochemical and petrological investigation of meteorite ablation products in till and ice of Antarctica [Ph.D. thesis]: Columbus, The Ohio State University, 525 p.
- Hein, A., Woodward, J., Marrero, S.M., Dunning, S.A., Steig, E.J., Freeman, S.P.H.T., Stuart, F.M., Winter, K., Westoby, M.J., and Sugden, D.E., 2016, Evidence for the stability of the West Antarctic Ice Sheet divide for 1.4 million years: Nature Communications, v. 7, 10325, doi:10.1038/ncomms10325.
- Joy, K., Fink, D., Storey, B., and Atkins, C., 2014, A 2 million year glacial chronology of the Hatherton Glacier, Antarctica and implications for the size of the East Antarctic Ice Sheet at the Last Glacial Maximum: Quaternary Science Reviews, v. 83, p. 46–57, doi:10.1016/j.quascirev.2013.10.028.
- Mackay, S.L., and Marchant, D.R., 2016, Dating buried glacier ice using cosmogenic ³He in surface clasts: Theory and application to Mullins Glacier, Antarctica: Quaternary Science Reviews, v. 140, p. 75–100, doi:10.1016/j.quascirev.2016.03.013.
- Mercer, J.H., 1983, Cenozoic glaciation in the Southern Hemisphere: Annual Review of Earth and Planetary Sciences, v. 11, p. 99–132, doi:10.1146/annurev.ea.11.050183.000531.
- Petit, J.R., et al., 1999, Climate and atmospheric history of the past 420,000 years from the Vostok ice core, Antarctica: Nature, v. 399, p. 429–436, doi:10.1038
- Scarrow, J.W., Balks, M.R., and Almond, P.C., 2014, Three soil chronosequences in recessional glacial deposits near the polar plateau, in the Central Transantarctic Mountains, Antarctica: Antarctic Science, v. 26, p. 573–583, doi:10 .1017/S0954102014000078.
- Sinisalo, A., and Moore, J.C., 2010, Antarctic blue ice areas—Towards extracting paleoclimate information: Antarctic Science, v. 22, p. 99–115, doi:10.1017 /S0954102009990691.
- Staiger, J.W., Marchant, D.R., Schaefer, J.M., Oberholzer, P., Johnson, J.V., Lewis, A.R., and Swanger, K.M., 2006, Plio-Pleistocene history of Ferrar Glacier, Antarctica: Implications for climate and ice sheet stability: Earth and Planetary Science Letters, v. 243, p. 489–503, doi:10.1016/j.epsl.2006.01.037.
- Sugden, D.E., Denton, G.H., and Marchant, D.R., 1993, The case for a stable East Antarctic ice sheet: The background: Geografiska Annaler, Series A: Physical Geography, v. 75, p. 151–154, doi:10.2307/521199.
- Sun, T., Socki, R.A., Bish, D.L., Harvey, R.P., Bao, H., Niles, P.B., Cavicchioli, R., and Tonui, E., 2015, Lost cold Antarctic deserts inferred from unusual sulfate formation and isotope signatures: Nature Communications, v. 6, 7579, doi: 10.1038/ncomms8579.
- Whillans, I.M., and Cassidy, W.A., 1983, Catch a falling star: Meteorites and old ice: Science, v. 222, p. 55–57, doi:10.1126/science.222.4619.55.

Manuscript received 28 March 2017 Revised manuscript received 12 July 2017 Manuscript accepted 13 July 2017

Printed in USA

Middle to late Pleistocene stability of the central East Antarctic Ice Sheet at the head of Law Glacier

M.R. Kaplan¹, K. Licht², G. Winckler^{1,3}, J.M. Schaefer^{1,3}, N. Bader², C. Mathieson¹, M. Roberts⁴, C.M. Kassab², R. Schwartz¹, and J. A. Graly²

This PDF file includes Materials and Methods, Figs. DR1 to DR5, and Tables DR1 to DR4

Sediment and moraine formation in the Mt. Achernar blue ice region

The first key point is that blue ice moraines are associated with blue ice areas, where sublimation dominates mass balance, as discussed in the main text (Whillans and Cassidy, 1983; Chinn, 1991, 1994; Cassidy et al., 1992; Sinisalo and Moore, 2010; Fogwill et al., 2011; Campbell et al., 2014; Hein et al., 2016). In Figures 1C and DR1A, the conceptual model of how such moraines form is based on extensive descriptions and concepts in these prior publications, and observations locally at Mt. Achernar (Scarrow et al., 2013; Bader et al., 2017). At this site, observations indicate that sediment entrained in and transported by the underlying ice is exposed at the surface over time via sublimation. On average 20% of pebbles on the moraine surface are faceted and/or striated suggesting a mix of basal and englacial transport (Bader et al., 2017).

The second key point is that the surface sediments overlie ice. The age progression implies that debris accretes laterally over time, which is consistent with the provenance-based interpretation of Bader et al. (2017). The debris also thickens with time (Scarrow et al., 2013; Bader et al., 2017). Yet, in comparison to moraines directly overlying bedrock – as is typically the case for "non-blue ice moraines" – the sediment-moraine shown in Figures 1 to 3 overlies ice that remains contiguous with the active Law outlet glacier. Bader et al. (2017) inferred the innermost 1-2 km of sediment-moraine (clean) is still most actively connected to the Law Glacier and connecting debris.

Thus, at Mt. Achernar, major changes in the elevation of the Law (and contiguous EAIS) glacier surface would be expected to alter markedly the flow in the ice underlying the sediment-moraines. For example, increases in ice elevation (thickening of Law Glacier) eventually may deform the moraine bands as observed in other areas (Chinn, 1991, 1994). For comparison, large decreases in ice elevation (thinning of Law Glacier) would result in reversal of flow and carry the surficial moraine out of the area.

At Mt. Achernar, not only are the bands quasi-continuous, mimicking the present moraine-active ice boundary, but there are bands of discrete petrologic compositions for several kilometres in places (Bader et al., 2017); these are visible in Figures 2 and DR3. Thus, we infer that the relatively undeformed nature of the moraine bands (including compositional bands) at Mt. Achernar reflects a long-lasting stability of ice flow from the respective ice sources.

¹Division of Geochemistry, Lamont-Doherty Earth Observatory, Palisades, NY 10964, USA

²Department of Earth Sciences, IUPUI, Indianapolis, IN 46202

³Department of Earth and Environmental Sciences, Columbia University, New York, NY 10027, USA

⁴2 Finch Street, Albert Town, Wanaka, New Zealand

Bader et al. (2017) also discussed in detail other changes in moraine morphology and sediment provenance (Fig. DR1A). For example, they documented that relatively minor changes indeed occurred in ice behaviour (<40 m surface elevation), as shown in Figure 3 and discussed in main text of this paper. However, such changes were not enough to deform or drain the blue ice moraine at Mt. Achernar (Chinn, 1991, 1994). Based on the evidence, Bader et al. (2017) concluded the Law Glacier has tapped into and eroded successively lower stratigraphic units of the Beacon Supergroup (Fig. DR1A).

Last, on sunny days, minor amount of supraglacial melting was observed. The melting appears to be associated with the dark debris, especially near the boundary between the moraine and clean Law Glacier (Fig. DR2E). Also, a minor amount of melting was observed in the youngest (10³ time scale) zone during the 2016/2017 austral summer. The relationship between melting and boulder/clast history, if any, is not yet clear.

Cosmogenic nuclide data

In austral summer 2010/2011, we collected quartz bearing sandstones and pyroxene bearing dolerites that appeared relatively stable (Figs. DR1, DR2). For example, we preferentially selected boulders away from hummocks. If necessary, we sampled the top of a hummock. We also preferred large table-shaped rectangular boulders (Fig. DR2); the idea is that although such boulders may have shifted somewhat, they are less likely to have completely flipped over, exposing a new side. Shifting of boulders could lead to ages being minima for when they arrived at the surface.

Samples were collected close to the topographic profile shown in Figure 2 (or DR4), which was the focus of provenance study in Bader et al. (2017). All samples were collected within ~500 m of the profile. The profile was taken with a rover GPS backpacking system. We note that samples MAR-11-23 and -30 are indeed on two different ridges, separated by a depression, as shown on Figure 3 (DR4), although they may appear to be on the same ridge given the scale of Figure 2B.

Samples were taken from the upper 1-3 cm from the most stable-looking flattish section, and if possible the center, of the boulder's top surface. Samples were collected with hammer and chisel. The azimuthal elevations of the surrounding landscape were measured using a compass and clinometer. We used a Trimble GPS system relative to the WGS 1984 datum to measure position including altitudes. All measurements were corrected differentially using continuous data from a base station set up at a semi-permanent camp for the field season. Post-processed uncertainties (1 σ) are <1 m for latitude-longitude and altitudes.

Regarding geologic effects on ages, first all ages assume no erosion. As Antarctica has some of the lowest erosion rates on Earth, this is negligible on the time scale discussed here. Some of the boulders are still striated (e.g., MAR-11-18, \sim 6-5 ka). Nonetheless, we point out that if we assume an erosion rate of \sim 10 cm Ma⁻¹, the 5 ka and 550 ka ages (youngest and oldest) increase by <5 years and \sim 5%, respectively; an erosion rate of 20 cm Ma⁻¹ causes an increase of by <5 years (0.08%) and \sim 10%, respectively. Also, we do not correct for snow cover on the boulders. We point out that this environment is one of the driest on Earth, and by definition blue ice areas contain generally little or no snow (Bintanja, 1999). Although some snow may accumulate in small depressions, we avoided such spots. On the other hand, Hagen (1995) noted 1 young outlier of \sim 15 ka could be explained by the fact it was collected from a depression with snow (Fig. 2A).

¹⁰Be, ²⁶Al

Details of processing and age calculations are provided in Tables DR1 and DR2 and shown on Figures 2 and 3, DR3, and DR4. Samples were processed using standard methods (Schaefer et al., 2009) and measured at the Center for Accelerator Mass Spectrometry at Lawrence Livermore National Laboratory (CAMS-LLNL). For age calculations, we used the production rate published in (Kaplan et al., 2011), which is the closest to Antarctica, at ~50°S. This rate is statistically indistinguishable from the other Southern Hemisphere production rate, derived in New Zealand at ~43°S (Putnam et al., 2010).

3 He

Processing of pyroxene separates followed the procedure outlined in Bromley et al. (2014) and Eaves et al. (2015, 2016). Abundance and isotopic analyses are performed with a MAP215-50 noble gas mass spectrometer (e.g., calibrated with a known volume of a Yellowstone helium standard (MM)). Details of measurements are provided in Table DR4.

For simplicity, all ages presented in the main text do not account for noncosmogenic ³He in the samples. That is, the ages are presented with the assumption all ³He is cosmogenically produced. However, noncosmogenic helium components (nucleogenic and inherited [mantle-derived]) may contribute a statistically significant contribution to the youngest samples in the study area (see next paragraph).

We emphasize, though, that the assumption of no nucleogenic or inherited helium has no effect on our conclusions. The reasons include: (i) critically, the findings also rely on ¹⁰Be-²⁶Al ages (Figs. 2, 3). All three nuclides are in agreement that moraines steadily get older; (ii) any potential correction becomes smaller as the ³He age increases. By 100 ka, the noncosmogenic ³He component is at least an order of magnitude less than total ³He concentration: this estimate is based on the following. The two Ferrar dolerite samples that afford the youngest age (both ~6.7 ka), also can be used to estimate the upper limit for the concentration of noncosmogenic ³He (Fig. 2). If we subtract the (statistically identical) average ³He concentration of these two samples from the concentrations in all other Helium samples, it reduces their respective ages. These adjusted ages are shown in Figures DR3 and DR4, which are identical to Figures 2 and 3 in main text, except they assume there is a maximum of ~6700 years' worth of noncosmogenic ³He. This equates to a maximum of about $\sim 5 \times 10^6$ atoms/g at the latitude and elevation of the Mt. Archernar samples. A concentration on the order of ~5 x 10⁶ is consistent with other estimates for the noncosmogenic ³He component in the Ferrar Dolerite (e.g., Margerison et al, 2005). Moreover, we note that this correction for noncosmogenic helium overall brings the ¹⁰Be-²⁶Al ages and ³He ages in closer agreement for the youngest dates.

Other systematic uncertainties

For 10 Be- 26 Al- 3 He age calculations we used the methods incorporated in the CRONUS-Earth online exposure age calculator version 2.2, with version 2.2.1 of the constants file (Balco et al., 2008; with a 10 Be half-life of 1.39 Ma, [Nishiizumi et al., 2007]). Taken at face value, uncertainties for the production rate are $\sim 3\%$ and $\sim 8\%$ for 10 Be- 26 Al and 3 He, respectively (Putnam et al., 2010; Kaplan et al., 2011).

At present, there are different scaling schemes available for position and elevation (Table DR2). We elected to use Lal (1991)/Stone (2000) scaling scheme, but note that the choice of has no effect on our findings. ³He and ¹⁰Be/²⁶Al ages will both change systematically if a different

production rate (Putnam et al., 2010; Kaplan et al., 2011) and scaling scheme are used (e.g., on Figs. 2, DR3).

With regards to the long term, for example, 10⁵ year-time scale or oldest ages on Figure 2, we do not know if the production rate has changed significantly. However, we emphasize the following. First, long-term changes are likely to be reduced at 85°S, because one of the most important effects on *in situ* production is a change in the geomagnetic field. Changes in the field strength are most important at the lowest latitudes. Whereas, Mt. Achernar is close to the south geographic and geomagnetic pole. Second, such production rate changes would not affect our main conclusions.

Prior cosmogenic ages in Hagen (1995)

In one of the earliest cosmogenic dating studies in Antarctica, Hagen (1995) obtained a ¹⁰Be and ²⁶Al dataset (Fig. 2). All the data in Hagen (1995) were recalculated (Table DR3) based on the up-to-date cosmogenic nuclide systematics discussed above. Similar to the new data (Tables DR1 to DR2), all of the previously obtained ²⁶Al/¹⁰Be concentration ratios overlap with the constant exposure line (Fig. DR5). This result also supports our conclusion these subglacially-derived samples do not contain a complex exposure/burial history.

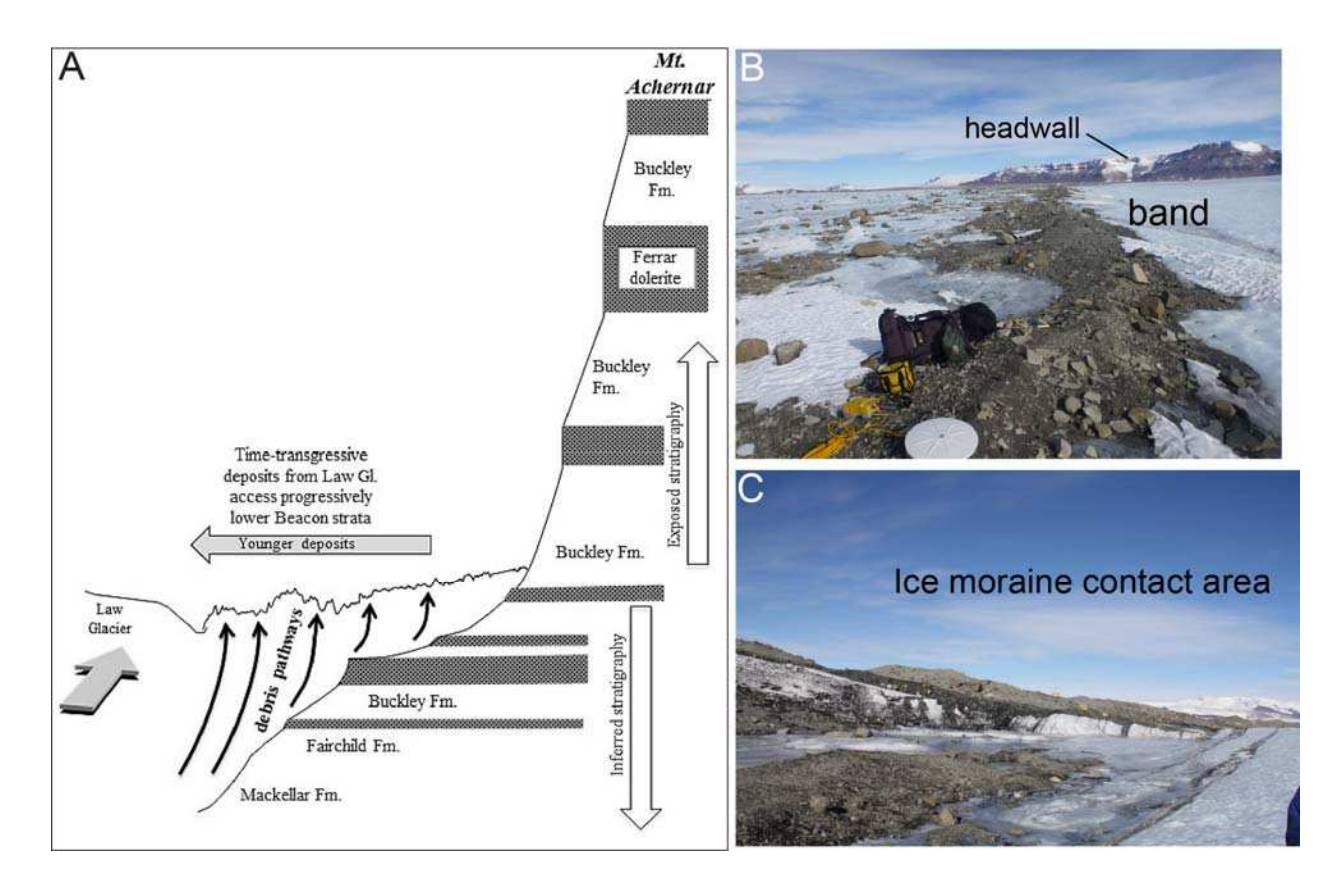


Figure DR1. A: From Bader et al. (2017). A conceptual model of blue ice moraine formation specifically at Mt. Achernar (cf., a more general model is in Figure 1C). The inferences in Figures 1C and DR1A are based on extensive descriptions in prior publications (Whillans and Cassidy, 1983; Cassidy et al., 1992; Fogwill et al., 2011; Chinn, 1991, 1994; Campbell et al., 2014; Hein et al., 2016; Bader et al. 2017). This figure shows the exposed 800 m thick bedrock (Faure and Mensing, 2010) and inferred (ice-covered) bedrock stratigraphy. Dark horizontal bands represent Ferrar dolerite sills, three of which are exposed. Black arrows show hypothesized debris transport pathways that explain the source of compositional changes in till across the moraine. This model highlights the sub- and englacial origin of the moraine sediment and spatio-temporal shift to debris sources lower in the bedrock stratigraphic section as new till accumulated toward what is the present-day Law Glacier margin. B: A photograph of the emerging debris band in the lower right of Figure 1B. Note that the substantial distance to the headwall (Mt. Achernar) indicates there is no local source of rockfall and the debris building up on the ice surface must be englacially or subglacially derived (cf., Fig. A). C) A photograph of a recently emerging band next to the ice-moraine boundary.

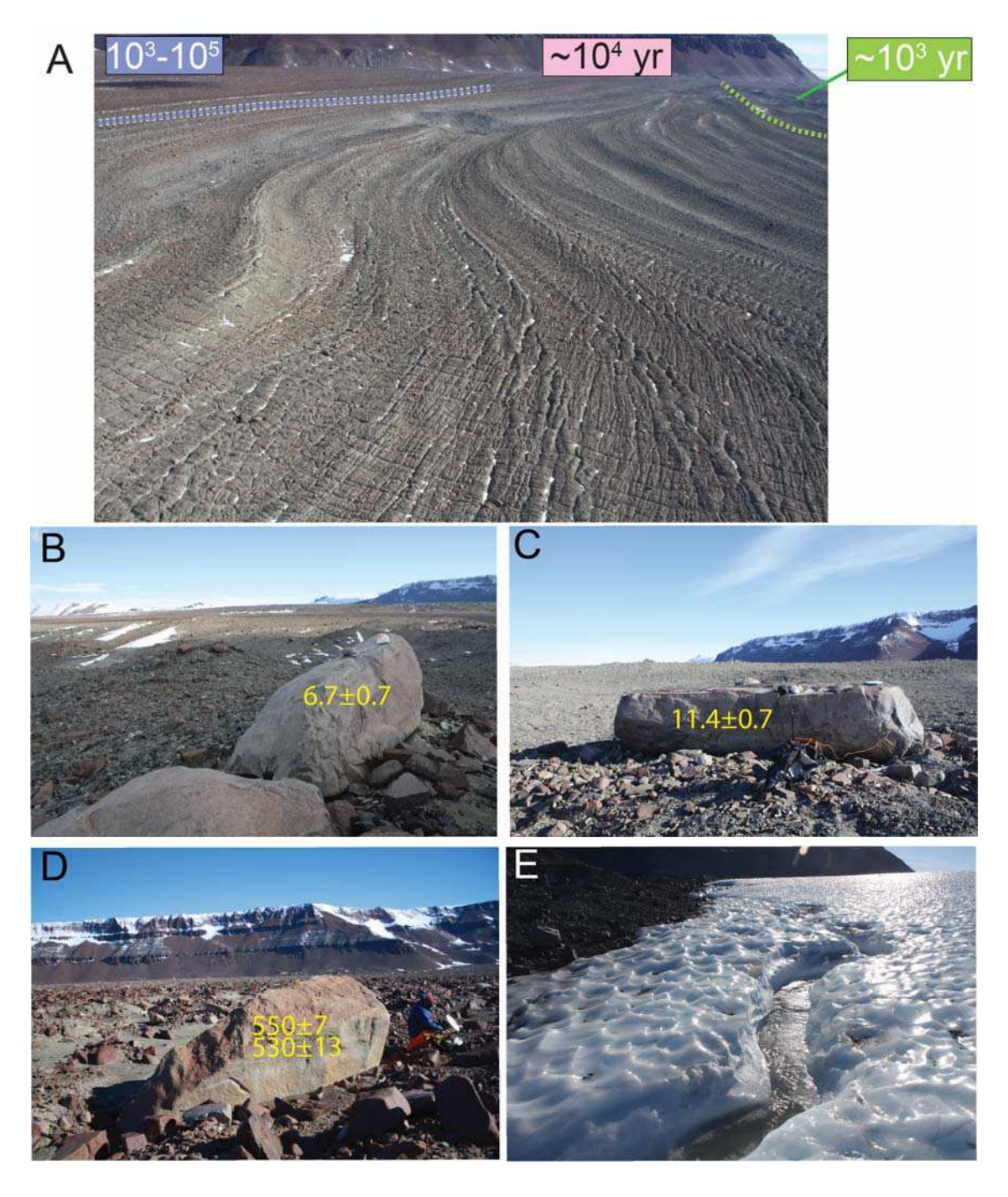


Figure DR2. A: Photo of the moraine, including ridges and depressions, at Mt. Achernar, with ages based on those shown in Figure 2. Note the increase in oxidation in the upper left. **B-D:** Photos of boulders with the youngest (B-C) and oldest (D) exposure ages. We tried to sample preferentially boulders with a flat table shape, if possible, given it may be more difficult for them to completely turn over (e.g., C). Note the oldest boulder (**D**) has the "most oxidized" top and it is surrounded by strongly oxidized material. In contrast, the younger samples shown in **B and C,** and their surroundings, lack the red oxidation of the older deposit. **E:** A photo that shows running water on the ice surface, January, 2011, indicating a minor amount of melting occurs in the summer close to where darker debris exists.

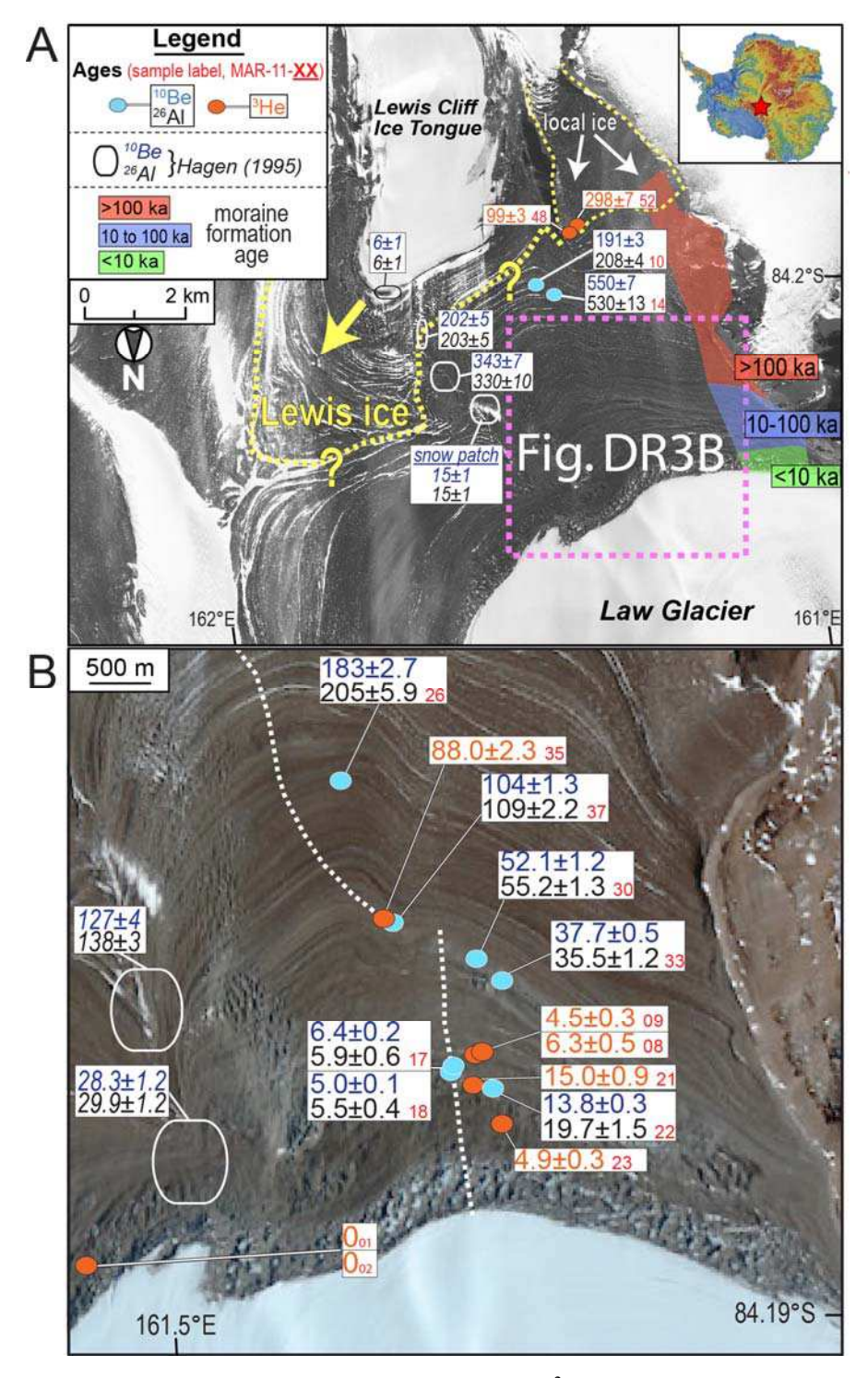


Figure DR3. Same as Figure 2, except assuming that each ³He measurement contains a maximum of 5.05 x 10⁶ atoms/g of noncosmogenic ³He (e.g., nucleogenic, magmatic), i.e., <6.7 ka equivalent age. This value is from the two youngest statistically identical samples, MAR-11-01 and 02, shown here in the lowermost left of panel B, and Figure 2B, and presented in Table DR4. This concentration was then subtracted from each sample's concentration, and the ages recalculated. The boundary between Law and Lewis ice is marked in yellow, which is uncertain in places (question mark). Dashed line in panel B represents profile in Figure DR4 (from Bader et al, 2017).

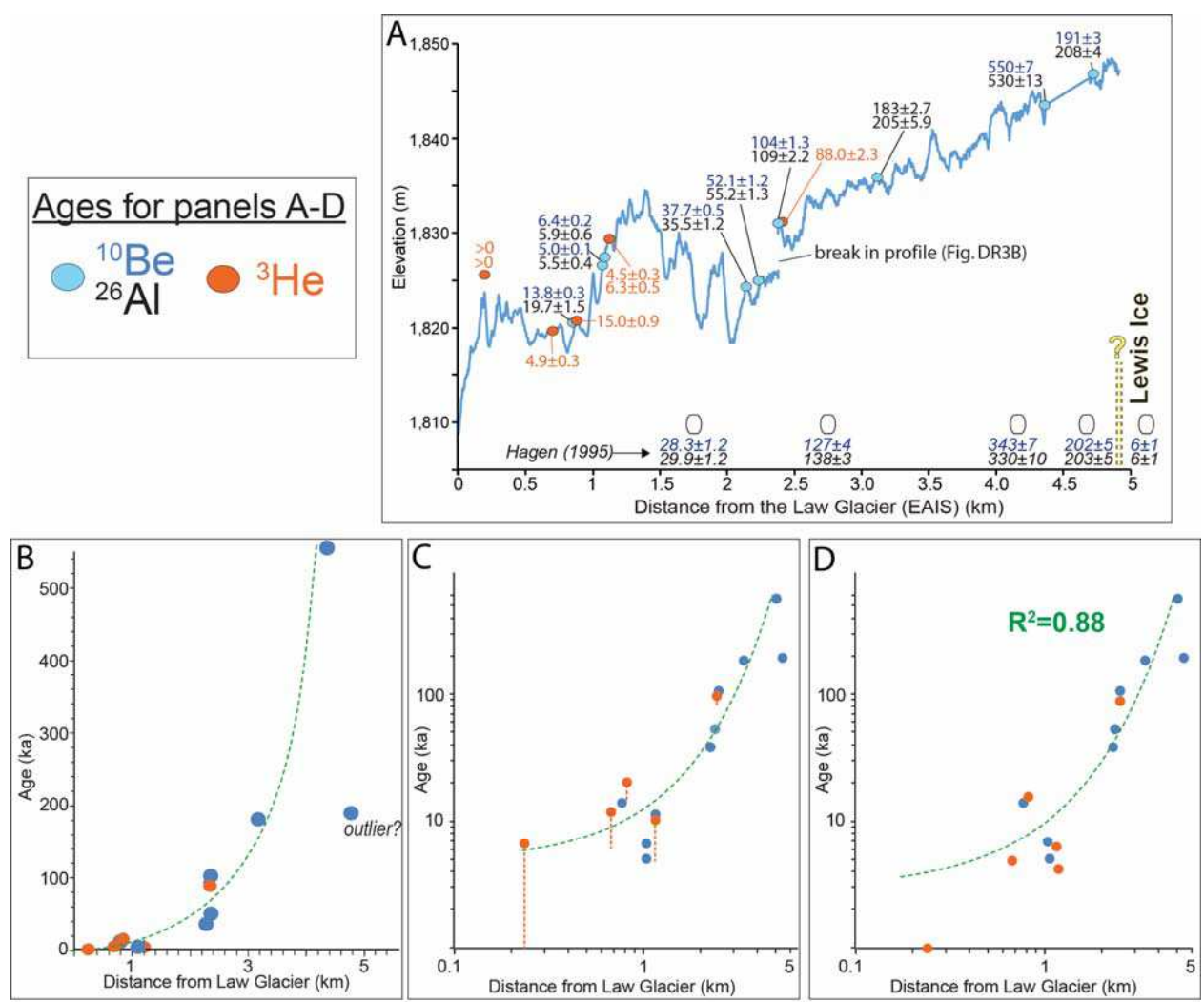


Figure DR4. Same as Figure 3, but following Figure DR3 above, it is assumed each 3 He measurement contains up to a maximum of 5.05×10^{6} atoms/g of noncosmogenic 3 He (nucleogenic or inherited, i.e., a maximum of 6.7 ka equivalent exposure 3 He age). This value is based on the two youngest samples, MAR-11-01 and 02 (Table DR4). This 3 He concentration is then subtracted from each sample's 3 He concentration (atoms/g), and then the 3 He ages are recalculated. As in Figure 2, it is assumed the \sim 190 ka 10 Be age from 5.6 km may be an outlier (see text).

Panels (A) and (B). Same as panels in Figure 3A and B in the main text but assuming each ³He age has a maximum of ~6.7 ka equivalent of noncosmogenic He. The profile is from Bader et a. (2017). (C) For comparison, same as Figure DR4B panel just to the left, except plotted on loglog axes. Dashed vertical red lines represent subtraction of ~6.7 ka equivalent age from each sample. Note the change is less as the samples increase in age. Once at 100 ka the ³He concentration in each sample is at least one order of magnitude higher than that in the 6.7 ka sample. (D) Same as Figure DR4C just to the left, except all ³He ages are shown with the subtracted value. Dashed green line is exponential fit, which is shown merely to illustrate the progressive age increase with distance from the Law Glacier. For simplicity of illustration, only ¹⁰Be and ³He ages are shown in B to D; however, the ²⁶Al data indicate the same result given overall age concordance.

The key point of these four panels is to show the agreement of all 3 nuclides that the moraines steadily get older with distance from the relatively clean surface of the Law Glacier margin.

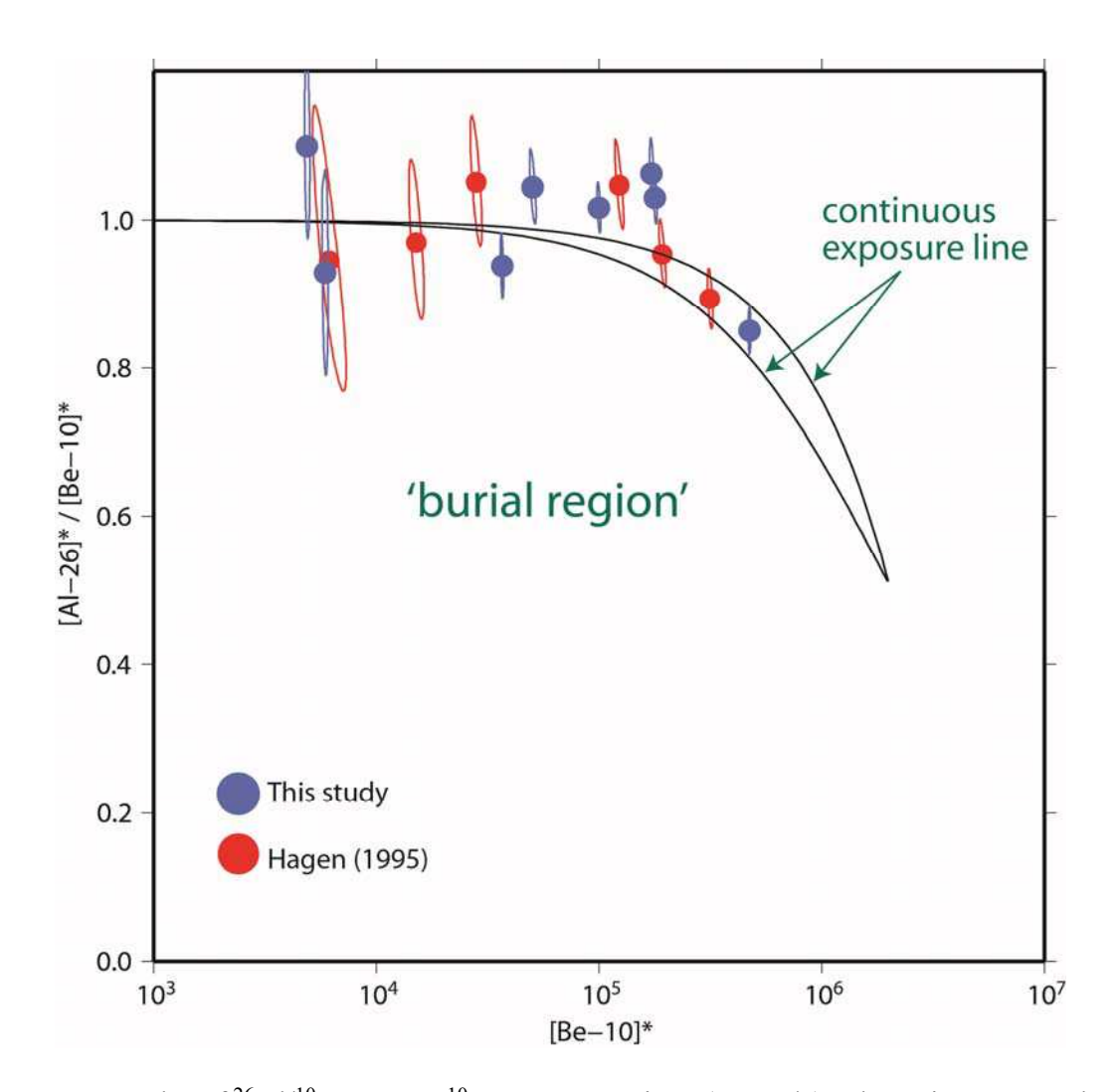


Figure DR5. A plot of 26 Al/ 10 Be versus 10 Be concentrations (atoms/g). The ratios are standardized (*) to 6.75, the Be-10 concentrations are relative to 07KNSTD and sea level high latitude (Balco et al., 2008). The plot indicates in a broad sense the samples do not indicate a complicated long-term history of exposure and burial (at least periods of burial greater than ~100,000 years). The data error envelops are 1σ analytical uncertainty.

Most ratios overlap with the continuous exposure line. 5 out of 15 ratios are slightly higher than the continuous exposure line, at 1σ (68% confidence level). However, 14 of 15 ratios overlap at 2σ (95% confidence level). The ratio of sample MAR-11-22 is not shown, as it lies above the plot. We are not sure of the reason 6 out of 15 samples, including MAR-11-22, provide slightly higher ratios (equivalent to >6.75 in Table DR1 below) at 1σ , than those represented along the continuous exposure line; especially, as most of the slightly-high ratio samples are in the first batch analyzed (Table DR1).

Table DR1. Surface-exposure sample details and ¹⁰Be and ²⁶Al data.

	Latitude	Longitude	Elevation	Sample	Shielding	Quartz	Carrier (Be)	Total (Al)
Sample ID	(DD)	(DD)	(masl) ^a	Thickness	correction	weight	Added	(g)
				(cm)		(g)	(g)	
MAR-11-22	-84.18863	161.26488	1831	0.61	0.9993	3.0517	0.1858	1.9849
MAR-11-10	-84.22163	161.35674	1860	1.07	0.9997	10.0921	0.1860	1.0860
MAR-11-18	-84.19057	161.28288	1834	1.05	0.9988	15.1808	0.1864	1.9681
MAR-11-26	-84.2086	161.34976	1847	1.67	0.9997	10.0372	0.1863	1.7343
MAR-11-30	-84.1980	161.26189	1847	1.07	0.9967	8.5678	0.1871	1.4846
MAR-11-37	-84.2008	161.3199	1843	1.36	0.9994	10.1317	0.1838	1.8284
BLANK_1_2012May					0.1861	1.0131		
BLANK_2_2012May					0.1836			
MAR-11-14a	-84.21938	161.33736	1859	2.02	0.9997	4.0553	0.1825	1.6752
MAR-11-14b	-84.21938	161.33736	1859	2.02	0.9997	4.0632	0.1838	1.6917
MAR-11-17	-84.19072	161.2820	1835	1.10	0.9988	5.0766	0.1862	1.2010
MAR-11-33	-84.1970	161.25064	1866	1.87	0.9990	8.092	0.1854	1.5731
Blank_2_2013Jan24							0.1777	1.4472

Sample ID	10 Be/ 9 Be $\pm 1\sigma^{b}$ 10^{-14}	$[^{10}\text{Be}] \pm 1_{\text{G}} (\text{atoms x g}^{-1})$ 10^{5}	$^{26}\text{Al}/^{27}\text{Al} \pm 1_{\text{O}}^{\text{b}}$ 10^{-14}	$[^{26}\text{Al}] \pm 1_{\text{G}} (\text{atoms x g}^{-1})$ 10^{5}	$^{26}\text{Al/}^{10}\text{Be}$ $\pm 1\sigma$
MAR-11-22	8.2612 ± 0.1843	3.3612 ± 0.0750	22.1414 ± 1.7538	32.1451 ± 2.5462	9.6 ± 0.8
MAR-11-10	363.7159 ± 5.2707	44.7971 ± 0.6492	1302.2702 ± 23.8240	312.7954 ± 5.7223	7.0 ± 0.2
MAR-11-18	14.6934 ± 0.2789	1.2057 ± 0.0229	31.0253 ± 2.3831	8.9783 ± 0.6896	7.4 ± 0.6
MAR-11-26	344.0529 ± 4.8424	42.6775 ± 0.6007	796.6776 ± 20.8441	307.2736 ± 8.0395	7.2 ± 0.2
MAR-11-30	85.7337 ± 2.0059	12.5134 ± 0.2928	229.0182 ± 5.3104	88.5792 ± 2.0539	7.1 ± 0.2
MAR-11-37	203.8014 ± 2.5791	24.7140 ± 0.3128	425.9514 ± 8.2534	171.5854 ± 3.3247	6.9 ± 0.2
BLANK_1_2012May01	0.0347 ± 0.0118		0.3601 ± 0.3601		5.7 ± 0.1
BLANK_2_2012May01	0.0314 ± 0.0105				5.8 ± 0.1
MAR-11-14a	390.8225 ± 4.2998	117.5487 ± 1.2933	725.8111 ± 13.5291	669.2379 ± 12.4746	6.3 ± 0.7
MAR-11-14b	387.3324 ± 4.2669	117.1206 ± 1.2902	734.4910 ± 13.7077	682.5808 ± 12.7389	6.3 ± 0.2
MAR-11-17	6.2607 ± 0.1874	1.5346 ± 0.0459	18.2125 ± 1.9192	9.6177 ± 1.0135	
MAR-11-33	59.0657 ± 0.7713	9.0480 ± 0.1181	131.9726 ± 4.4710	57.2676 ± 1.9401	
Blank_2_2013Jan24	0.2106 ± 0.0710		0.6938 ± 0.4907		

Note: Procedural blanks shown were processed identically to the samples, with one or two blanks accompanying each sample batch, respectively. ¹⁰Be/Be and ²⁶Al/Al ratios measured relative to 07KNSTD (2.85⁻¹²) and KNSTD standard (3.096⁻¹¹), respectively. Shown are analytical AMS uncertainties.

^aMeasured with a Trimble GPS system but undifferentiated cross checked with a handheld Garmin. ^bMAR-11-14 was measured twice to test reproducibility.

Table DR2. ¹⁰Be and ²⁶Al ages from Mt. Achernar.

Sample ID	10 Be Age $\pm 1\sigma$	26 Al Age $\pm 1\sigma$
	(yrs)	(yrs)
MAR-11-22	13800 ± 310	19700 ± 1570
MAR-11-10	191100 ± 2910	207600 ± 4210
MAR-11-18	5000 ± 100	5500 ± 420
MAR-11-26	182500 ± 2690	204700 ± 5930
MAR-11-30	52100 ± 1240	55200 ± 1320
MAR-11-37	103700 ± 1350	109300 ± 2240
MAR-11-14a	552300 ± 7000	517400 ± 12600
MAR-11-14b	555200 ± 7000	536700 ± 13200
MAR-11-17	6360 ± 190	5890 ± 620
MAR-11-33	37700 ± 500	35500 ± 1220

Note: 10 Be and 26 Al ages calculated using the Southern Hemisphere production rate in Patagonia at $\sim 50^{\circ}$ S (Kaplan et al., 2011) and methods discussed in (Balco et al., 2008), including the constant production rate model ('St' scaling scheme) of Lal (1991)/Stone (2000). Although we use the rate in Kaplan et al. (2011) because it is at a higher latitude, it is statistically identical to the other Southern Hemisphere production rate, obtained in New Zealand (Putnam et al., 2010) If other scaling schemes are used (Balco et al., 2008), this has no effect on our conclusions. Age uncertainties include internal analytical error only. Uncertainties for production rate are $\sim 3\%$. MAR-11-14 was measured twice to test reproducibility.

Table DR3. Surface-exposure sample details and ¹⁰Be and ²⁶Al data recalculated from Hagen (1995).

Sample	Lat.	Long.	Elevation	$[^{10}\text{Be}] \pm 1_{\sigma} (\text{atoms x g}^{-1})$	$[^{26}\text{Al}] \pm 1_{\sigma} \text{ (atoms x g}^{-1})$	10 Be Age $\pm 1_{\circ}$	26 Al Age $\pm 1_{\odot}$	26 Al/ 10 Be
ID	(DD)	(DD)	(m a.s.l.)	10 ⁵	10 ⁵	(yrs)	(yrs)	± 1σ
F-90-21	-81	161	1800	1.64 ± 0.19	9.49 ± 0.65	6170 ± 430	5840 ± 400	6.4 ± 0.9
F-90-18	-81	161	1800	51.22 ± 1.23	299.22 ± 6.58	202300 ± 5110	202500 ± 4900	6.5 ± 0.2
F-90-15	-81	161	1800	83.94 ± 1.56	459.4 ± 11.81	343200 ± 6960	330100 ± 10000	6.1 ± 0.2
F-90-14	-81	161	1800	4.03 ± 0.22	23.94 ± 1.29	15200 ± 830	14800 ± 800	6.6 ± 0.5
F-90-26	-81	161	1800	32.76 ± 1.02	209.88 ± 4.68	127000 ± 4080	137700 ± 3300	7.1 ± 0.3
F-90-27	-81	161	1800	7.47 ± 0.31	48.04 ± 1.82	28300 ± 1180	29900 ± 1200	$7.1~\pm~0.4$

Note: We round off latitude and longitude because Hagen (1995) did not provide coordinates (prior to handheld GPS systems). To consider this uncertainty in position, for Figure 2 (and DR3), we draw a \sim 1 km circle round the approximate area indicated in Hagen (1995). We use a sample thickness of 1 cm and we do not correct for topographic shielding, given no values were provided. We assume shielding is similar to the data in Table DR1. These approximations have no effect on our findings and conclusions.

¹⁰Be/Be and ²⁶Al/Al ratios measured relative to KNSTD standards (3.15⁻¹² and 3.096⁻¹¹, respectively). Shown are analytical AMS uncertainties. ^{26/10}Be ratios shown relative to 07KNSTD. Ages are calculated the same way as those in Table DR2.

Table DR4. Surface-exposure sample details and ³He data.

0 1 10	Latitude	Longitude	Elevation	Sample Thickness	Shielding	Pyroxene	$[^{3}\text{He}] \pm 1_{\sigma} (\text{atoms x g}^{-1})$	$He^3/He^4 \pm 1_{\odot}$	
Samp le ID	(DD)	(DD)	(m a.s.l.)	(cm)	correction	mass	10 ⁵	10^{-8}	He Age $\pm 1\sigma$
						(g)			
MAR-11-08(1)	-84.1910	161.2749	1829	1.07	0.999	0.0719	92.1456 ± 7.4858	8.6898 ± 1.1501	
MAR-11-08 (2)						0.0312	107.3186 ± 8.7819	11.3600 ± 0.9298	
				Ave	rage of the	2 analyses=	99.7321 ± 7.5865		12800 ± 970
MAR-11-23 (1)	-84.1870	161.2414	1825	1.35	0.999	0.0460	83.1669 ± 5.3854	10.8985 ± 0.8539	11400 ± 700
MAR-11-23 (2)						0.0371	93.9722 ± 6.8391	13.3016 ± 0.9684	
				Ave	rage of the	2 analyses=	88.5696 ± 5.4026		
MAR-11-52	-84.2286	161.2652	1830	1.09	0.999	0.0516	2380.1404 ± 55.2644	943.8149 ± 22.0226	304600 ± 7100
MAR-11-48 (1)	-84.2268	161.2755	1838	1.13	0.999	0.0254	823.7092 ± 22.4131	236.3370 ± 6.4346	104800 ± 2900
MAR-11-48 (2)						0.0263	828.0738 ± 22.7420	241.2585 ± 6.6291	105400 ± 2900
MAR-11-21 (1)	-84.1887	161.2672	1823	1.09	0.999	0.0285	176.8689 ± 9.4099	31.6898 ± 1.6862	22800 ± 1200
MAR-11-21 (2)						0.0333	155.7135 ± 8.1605	27.4441 ± 1.4385	20000 ± 1100
MAR-11-35	-84.2011	161.3220	1827	1.31	0.999	0.0315	735.4454 ± 19.5031	127.0875 ± 3.3719	94500 ± 2500
MAR-11-01	-84.1790	161.5365	1783	1.29	0.999	0.0290	50.2898 ± 4.4749	6.9904 ± 0.6221	6700 ± 590
MAR-11-02	-84.1791	161.5366	1785	0.57	0.999	0.0227	50.7600 ± 5.5215	10.4042 ± 1.1318	6700 ± 730
MAR-11-09	-84.1911	161.2725	1829	1.00	0.999	0.0262	85.2997 ± 5.9883	10.9323 ± 0.7676	10900 ± 770

Note: ³He ages calculated using global production rate in Goehring et al. (2010), which incorporates the mid-high Southern Hemisphere rate obtained in Ackert et al. (2003). This rate was recently confirmed by Eaves et al. (2015). Ages are based on 'St,' (same as ¹⁰Be-²⁶Al ages), the constant production rate scaling scheme (Lal, 1991/Stone 2000), although this has no effect on our conclusions. Age uncertainties include internal analytical error only.

MAR-11-08, MAR-11-23, MAR-11-48, and MAR-11-21 were each measured twice [(1) and (2)]: To test reproducibility between different preparers, MAR-11-48 and 21 were both processed twice, each time by a different person; the two respective analyses overlap at 1-2 σ analytical uncertainty, and we show an average age on all Figures. For MAR-11-08 and 23, we averaged two machine measurements on the same sample, which also overlap at 1σ analytical uncertainty.

Last, for Figures DR3 and DR4 above, the average of the identical concentrations in MAR-11-01 and MAR-11-02 is used as a maximum possible value for noncosmogenic component of ³He in. This amount potentially includes a magmatic component of ³He, although studies have shown this to be insignificant for the Ferrar dolerite (Ackert and Kurz, 2004).

REFERENCES

Ackert Jr., R.P., and Kurz, M.D., 2004, Age and uplift rates of Sirius Group sediments in the Dominion Range Antarctica, from surface exposure dating and geomorphology, Global and Planetary Change, v. 42, p. 207-225.

Ackert, R.P., Singer, B.S., Guillou, H., Kaplan, M.R., and Kurz, M.D., 2003, Calibration of ³He production rates against ⁴⁰Ar/³⁹Ar and K-Ar dated lava flows in Patagonia, Earth and Planetary Science Letters, v. 210, p. 119-136.

Bader, N.A., Licht, K.J., Kaplan, M.R., Kassab, C., and Winckler, G., 2017, East Antarctic Ice Sheet stability since the mid-Pleistocene recorded in a high-elevation ice-cored moraine, accepted pending minor revisions, Quaternary Science Reviews, v.159, p. 88-102.

Balco, G., Stone, J.O, Lifton, N.A., and Dunai, T.J., 2008, A complete and easily accessible

means of calculating surface exposure ages or erosion rates from 10Be and 26Al measurements, Quaternary Geochronology, v. 3, p. 174-195.

Bintanja, R., 1999, On the glaciological, meteorological and climatological significance of Antarctic blue ice area, Reviews of Geophysics, v. 37, p. 337-359.

Bromley, G.R.M., Winckler, G., Schaefer, J.M., Kaplan, M.R., 2014, Pyroxene separation by HF leaching and its impact on helium isotopes, Quaternary Geochronology, v. 23, p. 1-8.

Campbell S., Balco G., Todd C., Conway H., Huybers K., Simmons C., Vermeulen M., 2013, Radar-detected englacial stratigraphy in the Pensacola Mountains, Antarctica: implications for recent changes in ice flow and accumulation, Annals of Glaciology, v. 54, p. 91-100.

Cassidy, W., Harvey, R., Schutt, J., Disle, G., Yanai, K. 1992, The meteorite collection sites of Antarctica. Meteroritics, v. 27, p. 490-525.

Chinn, T.J., 1991, Polar glacier margin and debris features, Memorie della Societa Geologica Italiana, v. 46, p. 25-44.

Chinn, T.J., 1994, Glacier disequilibrium in the Convoy Range, Transantarctic Mountains, Antarctica, Institute of Geological & Nuclear Sciences Contribution 217, p. 269-276.

Desilets, D., and Zreda, M., 2003, Spatial and temporal distribution of secondary cosmic-ray nucleon intensities and applications to in-situ cosmogenic dating, Earth and Planetary Science Letters, v. 206, p. 21-42.

Dunai, T.J., 2001, Influence of secular variation of the magnetic field on production rates of in situ produced cosmogenic nuclides, Earth and Planetary Science Letters, v. 193, p.197-212.

Eaves, S.R., Winckler, G., Schaefer, J.M., Vandergoes, M.J., Alloway, B.V., Mackintosh, A.N., Townsend, D.B., Ryan, M.T., and Li, X., 2015, A test of the cosmogenic ³He production rate in the south-west Pacific (39°S), Journal of Quaternary Science, v. 30, p. 79-87.

Eaves, S.R., Mackintosh, A.N., Winckler, G., Schaefer, J.M., Alloway, B.V., Townsend, D.B., 2016, A Cosmogenic ³He chronology of late Quaternary glacier fluctuations in North Island, New Zealand (39°S), Quaternary Science Reviews, v. 132, p. 40-56.

Faure, G., Mensing, T.M., 2010, The Transantarctic Mountains: Rocks, Ice, Metorites, and Water. Springer Science by Business Media B.V. http://dx.doi.org/10.1007/978-90-481-9390-5_10, 289-469.

Fogwill, C.J., Hein, A.S., Bentley, M.J., and Sugden, D.E., 2011, Do blue-ice moraines in the Heritage Range show the West Antarctic ice sheet survived the last interglacial? Palaeogeography, Palaeoclimatology, Palaeoecology, v. 335-336, p. 61-70.

Goehring, B.M., Kurz, M.D., Balco, G., Schaefer, J.M., and Licciardi, J.M. and Lifton, N.A., 2010, A reevaluation of cosmogenic Helium-3 production rates, Quaternary Geochronology, v. 5, p. 410-18.

Hein, A., et al., 2016, Evidence for the stability of the West Antarctic Ice Sheet divide for 1.4 million years, Nature Communications, v. 7, p. 1-8.

Kaplan, M.R., Strelin, J.A., Schaefer, J.M., Denton, G.H., Finkel, R.C., Schwartz, R., Putnam, A.E., Vandergoes, M.J., Goehring, B.M., Travis, S.G., 2011, In-situ cosmogenic ¹⁰Be production rate at Lago Argentino, Patagonia: Implications for late-glacial climate chronology, Earth and Planetary Science Letters, v. 309, p. 21–32.

Lal, D., 1991, Cosmic-ray labeling of erosion surfaces in-situ nuclide production rates and erosion models, Earth and Planetary Science Letters, v. 104, p. 424-439.

Lifton, N., Smart, D., and Shea, M., 2008, Scaling time-integrated in situ cosmogenic nuclide production rates using a continuous geomagnetic model, Earth and Planetary Science Letters, v. 268, p. 190-201.

Margerison, H.R., Phillips, W.M., Stuart, F.M., Sugden, D.E., 2005, Cosmogenic ³He concentrations in ancient flood deposits from the Coombs Hills, northern Dry Valleys, East Antarctica: interpreting exposure ages and erosion rates, Earth Planetary Science Letters, v. 230, p. 163-175.

Nishiizumi, K., Imamura, M., Caffee, M.W., Southon, J.R., Finkel, R.C., and McAninch, J., 2007, Absolute calibration of ¹⁰Be AMS standards: Nuclear Instruments and Methods in Physics Research B, v. 258, p. 403-413.

Pigati, J.S., and Lifton, N.A., 2004, Geomagnetic effects on time-integrated cosmogenic nuclide production with emphasis on in situ ¹⁴C and ¹⁰Be, Earth and Planetary Science Letters, v. 226, p. 193-205.

Putnam, A., Schaefer, J., Barrell, D.J.A., Vandergoes, M., Denton, G.H., Kaplan, M., Finkel, R.C., Schwartz, R., Goehring, B.M., Kelley, S., 2010, In situ cosmogenic ¹⁰Be production-rate calibration from the Southern Alps, New Zealand, Journal of Quaternary Geochronology, v. 5, p. 392–409.

Scarrow, J.W., Balks, M.R., and Almond, P.C., 2014, Three soil chronosequences in recessional glacial deposits near the polar plateau, in the Central Transantarctic Mountains, Antarctica. Antarctic Science, doi:10.1017/S0954102014000078.

Schaefer, J.M., Denton, G.D., Kaplan, M. R., Putnam, A., Finkel, R.C., Barrell, D.J.A., Andersen, B.G., Schwartz, R. Mackintosh, A., Chinn, T., Schlüchter, C., 2009, High frequency glacier events in New Zealand during the Holocene are incoherent to the northern climate record, Science, v. 324, p. 622-625.

Sinisalo, A., and Moore, J.C., 2010, Antarctic blue ice areas – towards extracting paleoclimate information, Antarctic Science, v. 22, p. 99-115. Sinisalo, A, and Moore, J.C., 2010, Antarctic blue ice areas – towards extracting paleoclimate information, Antarctic Science, v. 22, p. 99-115.

Stone, J.O., 2000, Air pressure and cosmogenic isotope production: Journal Geophysical Research, v. 105, p. 23753-23759.

Whillans, I.M., and Cassidy, W.A., 1983, Catch a falling star: Meteorites and old ice, Science, v. 222, p. 55-57.